FABAD J. Pharm. Sci., 51, 3, 1285-1298, 2026
Doi: 10.55262/fabadeczacilik.1919333
RESEARCH ARTICLE

Optimization of pH-Triggered Endosomal Escape in Lipid Nanoparticles Using 3ß[L-Histidinamide-Carbamoyl] Cholesterol for Therapeutic Aptamer Delivery

Ozan KILIÇKAYA[*°], Cenk YILDIZ[**]

Optimization of pH-Triggered Endosomal Escape in Lipid Nanoparticles Using 3ß[L-Histidinamide-Carbamoyl] Cholesterol for Therapeutic Aptamer Delivery

SUMMARY

The intracellular delivery of therapeutic oligonucleotides is severely limited by the endosomal entrapment bottleneck. This study aims to resolve the "stability-fusogenicity paradox" through the rational design of pH-responsive lipid nanoparticles (LNPs) utilizing 3ß[L-histidinamide-carbamoyl] cholesterol (Hchol). Using Martini 2.2 coarse-grained molecular dynamics simulations (total 25 μs sampling), the Hchol-to-cholesterol ratio was systematically titrated while maintaining distearoylphosphatidylcholine (DSPC) at a constant 10% molar ratio. Results demonstrate that substituting 25% (F2) and 50% (F3) of the sterol fraction with Hchol triggers a morphological phase transition from a compact micellar core (Rg ≈4.61 nm) to stable vesicular-like geometries (Rg ≈11.4 nm) at endosomal pH 4.0. In contrast, 100% Hchol substitution (F5) led to catastrophic structural failure. Solvent accessible surface area (SASA) and mass density profiling confirmed that the AS1411 aptamer remained strictly sequestered within a protected internal water pool, preserving its functional G-quadruplex topology. Mechanistically, Hchol reduced the electrostatic grip of ionizable SM-102 lipids on the aptamer backbone by ~45%, acting as a "fusogenic primer" for the Vesicle Budding-and-Collapse (VBC) mechanism. Crucially, control simulations confirmed that F2 and F3 formulations maintain their robust architecture and absolute cargo protection at physiological pH (7.4). Our findings identify F2 and F3 as "Goldilocks" formulations that achieve an ideal balance between systemic structural integrity and enhanced endosomal escape potential. This framework provides a robust new platform for therapeutic aptamer encapsulation, intracellular delivery, and pH-responsive endosomal escape.

Keywords: *Lipid nanoparticle, hchol, AS1411 aptamer, molecular dynamics, endosomal escape.*

Terapötik Aptamer İletimi İçin 3ß-[L-Histidinamid-Karbamoil] Kolesterol Kullanılarak Lipid Nanopartiküllerde pH-Tetiklemeli Endozomal Kaçışın Optimizasyonu

ÖZ

Terapötik oligonükleotidlerin hücre içi iletimi, endozomal hapsolma darboğazı nedeniyle kısıtlıdır. Bu çalışma, 3ß[L-histidinamide-carbamoyl] kolesterol (Hchol) kullanarak pH duyarlı lipid nanopartiküllerin (LNP) rasyonel tasarımı yoluyla "stabilite-füzojenisite paradoksunu" çözmeyi amaçlamaktadır. Martini 2,2 kaba taneli moleküler dinamik simülasyonları (toplam 25 μs) kullanılarak, distearoilfosfatidilkolin (DSPC) oranı %10'da sabitlenirken Hchol/kolesterol oranı sistematik olarak titre edilmiştir. Bulgular, sterol fraksiyonunun %25 (F2) ve %50 (F3) oranında Hchol ile değiştirilmesinin, pH 4,0'da kompakt miseller yapıdan (Rg ≈4,61 nm) stabil veziküler benzeri geometrilere (Rg ≈11,4 nm) geçişi tetiklediğini göstermiştir. Öte yandan, %100 Hchol (F5) kullanımı katastrofik yapısal bozulmaya yol açmıştır. Solvent erişilebilir yüzey alanı (SASA) ve kütle yoğunluğu analizleri, AS1411 aptamerinin korunaklı bir iç su havuzunda başarıyla hapsedildiğini ve G-quadruplex yapısının korunduğunu doğrulamıştır. Mekanistik olarak Hchol, iyonize SM-102 lipidlerinin aptamer üzerindeki elektrostatik baskısını %45 oranında azaltarak sistemi "Vesicle Budding-and-Collapse" (VBC) mekanizması için hazırlamaktadır. Kritik olarak, kontrol simülasyonları F2 ve F3 formülasyonlarının fizyolojik pH'ta (7,4) sağlam yapılarını ve mutlak kargo korumalarını sürdürdüğünü doğrulamıştır. Çalışmamız, F2 ve F3 formülasyonlarının sistemik yapısal bütünlük ile endozomal kaçış potansiyeli arasında ideal dengeyi sağladığını ortaya koymaktadır. Bu sistem, terapötik aptamerlerin korunması, hücre içi iletimi ve pH duyarlı endozomal kaçışı için yenilikçi bir platform sunmaktadır.

Anahtar Kelimeler: *Lipid nanopartikül, hchol, AS1411 aptamer, moleküler dinamik, endozomal kaçış.*

Recieved: 31.03.2026
Revised: 26.08.2026
Accepted: 21.09.2026

[*] ORCID: 0000-0003-2710-2149, Afyonkarahisar Health Sciences University, Faculty of Pharmacy, Department of Pharmaceutical Biotechnology
[**] ORCID: 0000-0003-2672-8684, Afyonkarahisar Health Sciences University, Faculty of Pharmacy, Department of Pharmaceutical Technology

[°] Corresponding Author; Ozan Kılıçkaya
E-mail: ozan.kilickaya@afsu.edu.tr

INTRODUCTION

The emergence of nucleic acid-based therapeutics has fundamentally altered the landscape of modern pharmacology, offering precise molecular interventions for previously untreatable genetic disorders and malignancies (Kulkarni et al., 2021; Paunovska, Loughrey, & Dahlman, 2022). However, the clinical utility of these delicate macromolecules, such as mRNA, siRNA, and aptamers, is strictly governed by the efficiency of their delivery systems (Mitchell et al., 2020). Among various non-viral platforms, lipid nanoparticles (LNPs) have established themselves as the clinical gold standard, a status reinforced by the global success of COVID-19 mRNA vaccines and the approval of siRNA therapies like Onpattro (Cullis & Hope, 2017; Hou, Zaks, Langer, & Dong, 2021). Despite these milestones, current LNP technologies face a formidable biological bottleneck: endosomal entrapment. Research indicates that less than 5% of the internalized LNP cargo successfully escapes the endo-lysosomal pathway to reach the cytoplasm, while the majority is subjected to enzymatic degradation or exocytic recycling (Gilleron et al., 2013; Pei, 2025).

A canonical LNP architecture comprises four distinct lipid classes: ionizable lipids, sterols, PEGylated lipids, and structural phospholipids (Schoenmaker et al., 2021). Each component plays a non-redundant role in the nanoparticle's lifecycle. While ionizable lipids are the primary drivers of encapsulation and endosomal disruption, distearoylphosphatidylcholine (DSPC) is critical for maintaining the "structural status" and phase behavior of the particle (Eygeris, Patel, Jozic, Sahay, & Sahay, 2020; Suzuki & Ishihara, 2021). Incorporated at a strategic 10% molar ratio, DSPC provides necessary rigidity and bilayer stability, preventing premature cargo leakage and aggregation in the systemic circulation (Kulkarni, Witzigmann, Leung, Tam, & Cullis, 2019). Nevertheless, the traditional inclusion of cholesterol as a passive structural filler has recently been challenged in favor of stimuli-responsive analogs that can actively participate in overcoming biological barriers (Patel et al., 2020).

A promising innovation in this domain is the development of 3β[L-histidinamide-carbamoyl] cholesterol (Hchol), an ionizable helper lipid designed to replace or augment conventional cholesterol (Cheng et al., 2018; Jung et al., 2024). Hchol features an imidazole headgroup with a *pKa* value near 6.0, which remains predominantly neutral at physiological pH (7.4) but becomes significantly protonated within the acidic microenvironment of maturing endosomes (pH 5.5–6.0) (Han et al., 2021). This pH-triggered ionization is hypothesized to induce a "proton sponge" effect or facilitate the more recently proposed vesicle budding-and-collapse (VBC) mechanism, thereby enhancing membrane destabilization and cytosolic release efficiency (Pei, 2025; Vermeulen, De Smedt, Remaut, & Braeckmans, 2018). Furthermore, the integration of Hchol must be balanced with the structural scaffold provided by DSPC to ensure that the increased fusogenicity does not compromise the overall integrity of the delivery vehicle (Miao et al., 2019; Suzuki & Ishihara, 2021).

While therapeutic oligonucleotides such as the AS1411 G-quadruplex aptamer exhibit potent antineoplastic activity by interfering with nucleolin-mediated oncogenic pathways (Bates, Laber, Miller, Thomas, & Trent, 2009; Wei, Zhou, Wang, Wang, & Chen, 2022; Zhu & Chen, 2018), their therapeutic potential is severely bottlenecked by endo-lysosomal entrapment (Sahay, Alakhova, & Kabanov, 2010). Cytosolic delivery is fundamentally futile if the internalized nucleic acid cargo cannot escape endosomal vesicles to reach its intracellular targets. Furthermore, current efforts to optimize LNP performance frequently rely on ad hoc lipid substitutions that inadvertently destabilize the nanoparticle architecture. Thus, a critical formulation paradox persists; modifications that enhance endosomal fusogenicity frequently compromise the systemic stability of the nanocarrier (Donahue, Acar, & Wilhelm, 2019; Hassett et al., 2019).

To address the acute need for structurally rigorous, high-efficiency delivery vehicles, this study details the

rational design of a pH-responsive LNP framework tailored for the stable encapsulation and cytosolic release of the AS1411 aptamer as a therapeutic cargo. We propose a formulation platform combining the structural protection of tertiary nucleic acid architectures with the pH-triggered escape dynamics of Hchol. Crucially, we investigate a systematic titration of the Hchol/conventional cholesterol ratio while deliberately locking the structural lipid DSPC at a 10% molar ratio to resolve the stability-fusogenicity paradox. Through this approach, we aim to provide a robust paradigm for therapeutic aptamer encapsulation and endosomal delivery.

MATERIALS AND METHODS

Coarse-grained mapping and force field parameters

All computational simulations were conducted utilizing the Martini 2.2 coarse-grained (CG) force field (De Jong et al., 2013), which provides a highly optimized framework for investigating the self-assembly and phase behavior of lipidic systems over extensive spatiotemporal scales. The tertiary structure of the AS1411 aptamer was obtained from the Protein Data Bank (PDB ID: 2N3M) (Burley et al., 2017) and mapped to the CG resolution, preserving its native G-quadruplex folding topology (Van den Avont & Sharma-Walia, 2023). To mimic the acidic microenvironment (pH 4.0) prevalent during the microfluidic/ethanol injection synthesis process and early endosomal maturation, the ionizable headgroups of the specific lipids were explicitly protonated. Consequently, the tertiary amine of the SM-102 lipid was assigned a net charge of +1.0 *e*. Similarly, the imidazole ring of the newly introduced helper lipid, 3β[L-histidinamide-carbamoyl] cholesterol (Hchol), was modeled in its cationic state (+1.0 *e*) to simulate its pH-responsive fusogenic activity. Conventional structural lipids, including 1,2-distearoyl-sn-glycero-3-phosphocholine (DSPC), cholesterol (CHOL), and DMG-PEG2000 (DPEG), were parameterized using standard Martini lipid topologies.

LNP formulation and systematic titration strategy

To elucidate the structural and functional impact of Hchol, a systematic titration matrix was designed based on a clinically validated baseline molar ratio of 50:10:38.5:1.5 (ionizable lipid:phospholipid:sterol:PEG-lipid) (Schoenmaker et al., 2021). A constant molecular count of 500 SM-102, 100 DSPC, and 15 DPEG molecules were maintained across all systems. The total sterol fraction (38.5 mol%, corresponding to 385 molecules) was fractionally substituted with Hchol to generate five distinct formulations (Table 1.).

Table 1. Physical parameters of LNP formulations at endosomal pH 4.0. The percentages represent fractional substitutions within the total sterol content, not the entire LNP formulation

Formulation	Cholesterol Ratio / Number of Molecules	Hchol Ratio / Number of Molecules
F1	100% / 385 molecules	0% / no molecules
F2	75% / 289 molecules	25% / 96 molecules
F3	50% / 193 molecules	50% / 192 molecules
F4	25% / 96 molecules	75% / 289 molecules
F5	0% / no molecules	100% / 385 molecules

System assembly and solvation

A single AS1411 aptamer was positioned at the center of a cubic simulation box with exceedingly large dimensions (30x30x30 nm^3). This extensive box volume was deliberately chosen to ensure an "infinite dilution" condition, preventing periodic boundary artifacts and allowing the lipid mixture to self-assemble naturally into a thermodynamically stable, isotropic spherical geometry rather than forced lamellar or cylindrical phases. The constituent lipids for each formulation were randomly inserted into the simulation box. The system was subsequently solvated with approximately 100,000 Martini water beads. To achieve physiological electroneutrality, the net charge of the

system (dictated by the AS1411 backbone, protonated SM-102, and Hchol variants) was balanced by the systematic addition of standard physiological counter-ions (Cl^- or Na^+).

Molecular dynamics simulation protocol

All simulations were executed using the GROMACS 2025 software package (Abraham et al., 2015), fully hardware-accelerated via NVIDIA CUDA technology. Initial steric clashes and unfavorable contacts within the randomly assembled mixtures were resolved using the steepest descent energy minimization algorithm (5,000 steps). Following minimization, an extensive 1.0 μs (1000 ns) production run was performed for each formulation under the isothermal-isobaric (NPT) ensemble. To replicate the thermal conditions of the nanoparticle formulation process, the system temperature was strictly maintained at 333 K (60 °C) using the V-rescale thermostat (Bussi, Donadio, & Parrinello, 2007) with a coupling constant (τ_t) of 1.0 ps. The pressure was isotropically regulated at 1.0 bar using the C-rescale barostat (τ_p = 12.0 ps, compressibility = 3 x 10^{-4} bar^{-1}). The equations of motion were integrated using a 20-fs time step. Non-bonded electrostatic and van der Waals interactions were calculated utilizing the Reaction-Field method with a 1.1 nm cutoff. To ensure robust statistical significance and reproducibility, the entire 1.0 μs trajectory for each of the five formulations was independently replicated five times (n = 5), each initialized with a different random velocity seed, resulting in a total aggregated sampling time of 25 μs.

Simulation protocol and parameterization at physiological pH (7.4)

To evaluate systemic stability and confirm cargo retention during systemic circulation, parallel control simulations were performed for the leading formulations (F2 and F3) under physiological conditions (pH 7.4). At pH 7.4:

- SM-102: Modeled in its uncharged, deprotonated state (net charge = 0.0 e), consistent with its apparent pKa (~6.5–6.7).
- Hchol: The imidazole headgroup (pKa ~6.0) was modeled in its neutral form (net charge = 0.0 e).
- DSPC and DPEG: Retained standard neutral and zwitterionic Martini 2.2 parameters.
- AS1411 Aptamer: Modeled with its fully ionized polyanionic backbone (-1.0 e per nucleotide bead).
- Solvation & Counter-ions: Systems were solvated with standard Martini water and neutralized using physiological Na^+ counter-ions. Trajectories were generated using the same NPT ensemble parameters (T = 333 K, P = 1.0 bar, 1.0 μs duration, n = 5 independent replicates per formulation).

Trajectory analysis and biophysical characterization

To construct continuous molecular trajectories, periodic boundary conditions (PBC) were rigorously corrected post-simulation. The temporal stability, morphological evolution, and encapsulation efficiency of the LNPs were quantitatively assessed using intrinsic GROMACS utilities.

- Structural Integrity: Analyzed via the Radius of Gyration (R_g), focusing on individual axial components (R_{gx}, R_{gy}, R_{gz}) to confirm spherical symmetry.
- Encapsulation Efficiency: Evaluated through the continuous measurement of the Aptamer's Solvent Accessible Surface Area (SASA).
- Core-Shell Architecture: Mapped utilizing radial mass density profiling from the center of mass.
- Molecular Interactions: Characterized by calculating the Radial Distribution Function (RDF) and the time-resolved atomic contact number (< 0.6 nm) between the aptamer and ionizable lipids.
- Cargo Stability: Monitored via the Root Mean Square Deviation (RMSD) and Root Mean Square Fluctuation (RMSF) of the AS1411 backbone. All quantitative data are reported as the ensemble average ± standard deviation across the five independent replicates. High-fidelity molecular visualizations and cross-sectional density renderings were generated using PyMOL 3.0 (Yuan, Chan, & Hu, 2017).

RESULTS AND DISCUSSION

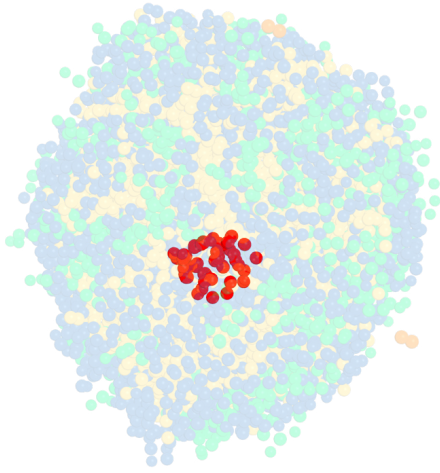

Figure 1. Detailed Cross-Section of the Control Lipid Nanoparticle (F1, 0% Hchol) at Endosomal pH 4.0. AS1411 is shown as red dots

The spherical LNP is shown cut in half to expose its internal architecture (Figure 1.). The semi-translucent lipid shell forms a stable, fused barrier (R_g = 4.6 nm). A dynamic internal water pool is sequestered within this shell. Most critically, the folded AS1411 aptamer (coarse-grained beads: opaque ruby-red spheres) is perfectly compartmentalized at the thermodynamic center of the nanoparticle, insulated by the dense core water pool, which provides continuous, hydrophobic armor against external solvent exposure and degradation.

Morphological evolution and phase transition of LNPs

To determine the impact of the pH-responsive Hchol lipid on the macroscopic structural integrity of the nanoparticles, the dynamic evolution of the LNP morphology was monitored over 1.0 s using the R_g. The structural phase behavior of the LNPs exhibited a profound dependency on the sterol composition, as depicted in Figure 2.

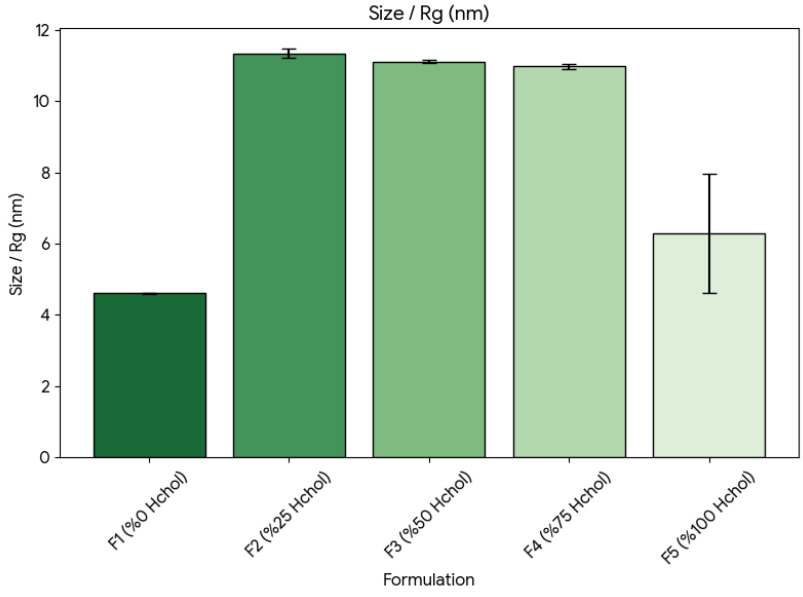

Figure 2. Time evolution of the R_g for LNP formulations (F1-F5) over 1.0 **µs**, illustrating structural phase transitions

The control formulation (F1, 0% Hchol) rapidly assembled into a highly compact and thermodynamically stable micellar core, maintaining a uniform *Rg* of 4.61±0.01 nm across all five independent replicates. Interestingly, the introduction of 25% Hchol (F2) triggered an immediate structural phase transition. The competitive integration of the bulky, protonated imidazole headgroups of Hchol disrupted the tight micellar packing, driving the system to expand into a stable, larger vesicular-like architecture with an *Rg* of 11.34±0.12 nm. This stable expansion was consistently observed in formulations F3 (50% Hchol) and F4 (75% Hchol). However, complete substitution with the ionizable sterol (F5, 100% Hchol) resulted in critical structural destabilization, with individual replicates fluctuating erratically between ~5.1 nm and 8.8 nm. This indicates that a baseline ratio of structural sterols is strictly required to mitigate catastrophic vesicle collapse.

Conformational stability and shielding of the aptamer cargo

While macroscopic phase transitions and volumetric expansions were observed across the Hchol titration matrix, the protective efficacy of the internal LNP core was quantitatively assessed via the SASA.

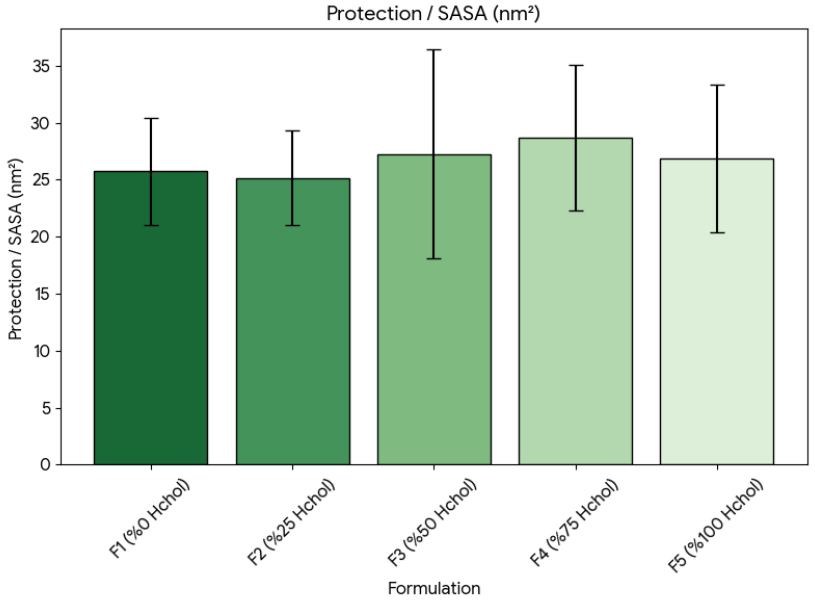

Figure 3. SASA of the encapsulated AS1411 aptamer, demonstrating consistent solvent shielding across stable formulations

Despite the drastic dimensional expansion observed in the F2, F3, and F4 systems, the SASA of the aptamer remained tightly constrained within a highly conserved range of 25.15 to 28.66 nm² (Figure 3.). To further corroborate these SASA findings, the internal cross-sectional mass density profile of the LNP core was analyzed (Figure 4.).

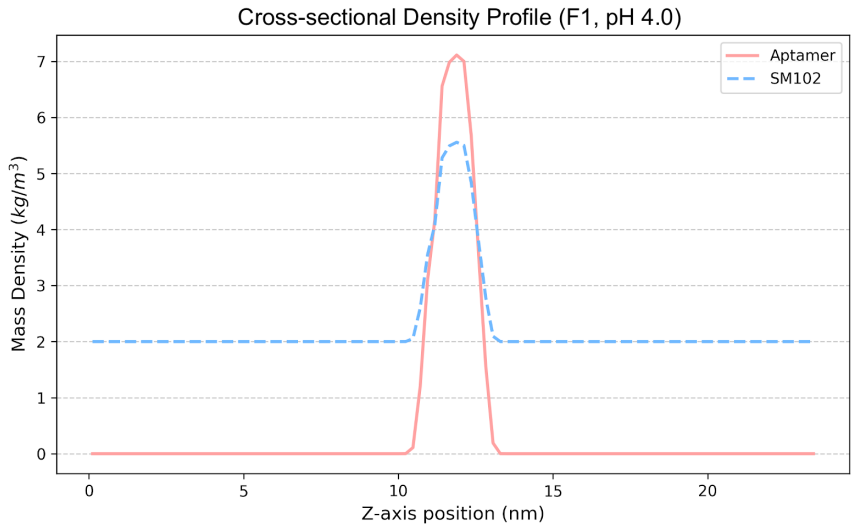

Figure 4. Cross-sectional mass density profile of the LNP, highlighting the dense packing of the aptamer at the center of mass

In the control formulation, the encapsulated aptamer exhibited a highly concentrated mean peak density of 7.52±0.41 kg/m³ exactly at the center of mass. Remarkably, this central peak density remained strictly conserved across all stable Hchol titrations. As detailed in Figure 5, this spatial density conservation mathematically proves that the internal water pool remains tightly sealed and the cargo remains densely packed, even as the overarching macroscopic volume of the nanoparticle expands.

This spatial density conservation mathematically proves that the internal water pool remains tightly sealed, and the cargo remains densely packed, even as the overarching macroscopic volume of the nanoparticle expands.

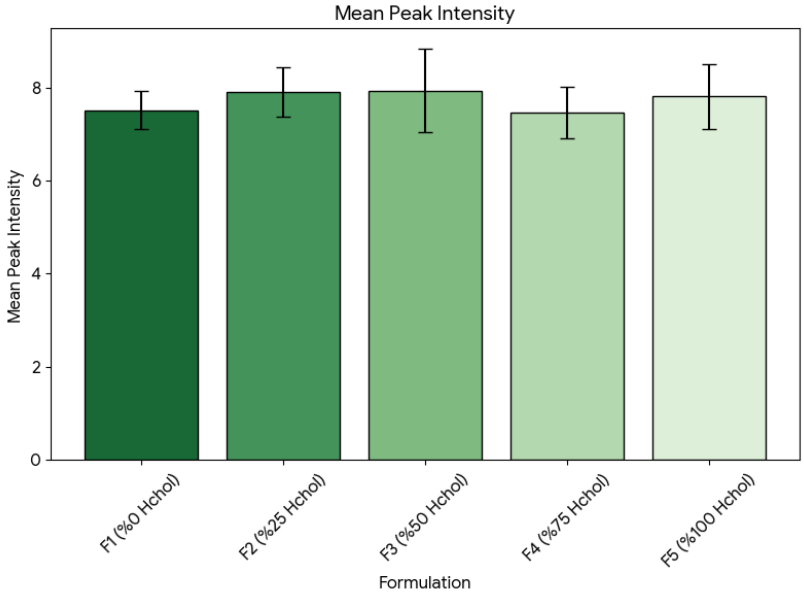

Figure 5. Mean Peak Mass Density across varying Hchol titrations

The structural integrity of the encapsulated AS1411 aptamer was further evaluated using RMSD and RMSF.

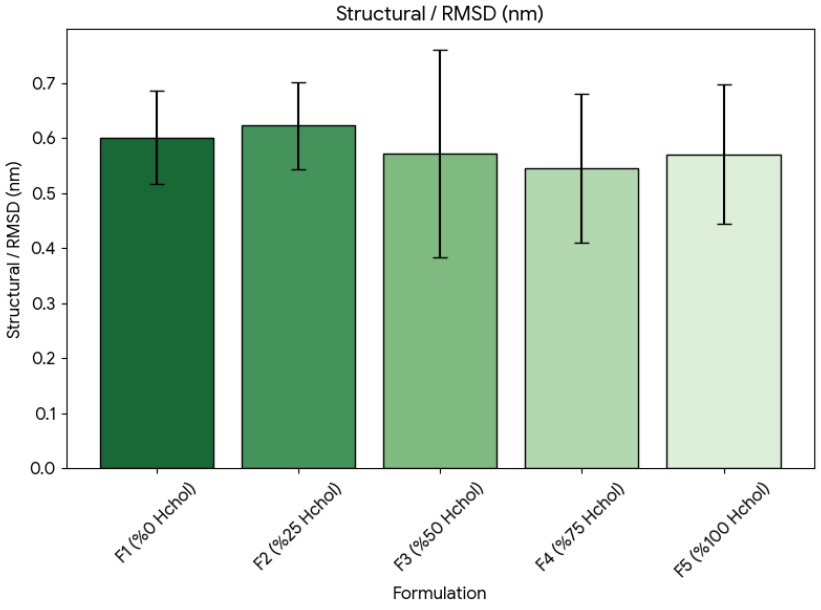

Figure 6. RMSD analysis of the AS1411 aptamer topology

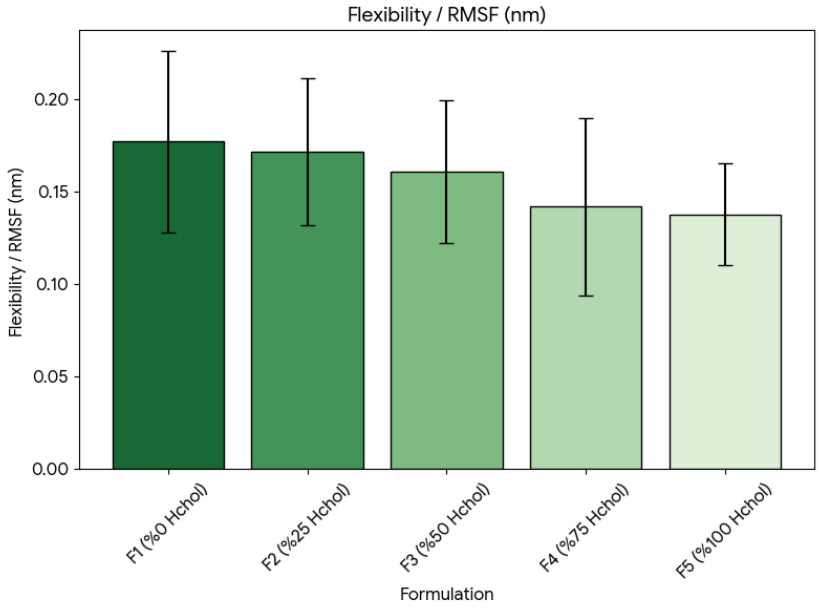

Figure 7. RMSF of the aptamer nucleotides, showing local structural flexibility

Across all evaluated formulations, the aptamer rapidly reached a stable equilibrium, with ensemble-averaged RMSD values strictly plateauing around ~0.60 nm (Figure 6.). The RMSF analysis (Figure 7.) similarly showed that local nucleotide fluctuations remained minimal (0.14 - 0.18 nm). These minimal structural deviations confirm that neither the intense initial lipid packing nor the subsequent Hchol-induced vesicular expansion induces deleterious unfolding or denaturation of the native G-quadruplex topology.

Electrostatic remodeling and priming for endosomal escape

To elucidate the mechanistic role of Hchol in enhancing fusogenicity at the endosomal pH (4.0), the specific electrostatic interactions between the negatively charged AS1411 aptamer and the cationic SM-102 ionizable lipids were quantitatively mapped using the RDF.

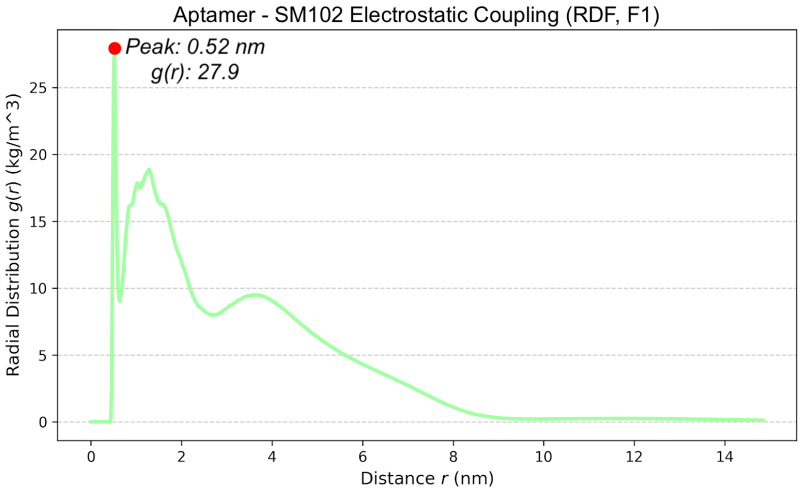

Figure 8. RDF between the cationic SM-102 headgroups and the anionic aptamer backbone

In the control formulation (F1), the protonated SM-102 molecules exhibited a profound electrostatic affinity for the aptamer backbone, evidenced by a sharp, highly localized RDF peak at exactly 0.52 nm with a maximum g(r) value of 28.65±3.54 (Figure 8.). Upon the systematic titration of Hchol, the RDF peak intensity was nearly halved in the F2 and F3 formulations, indicating a controlled attenuation of these electrostatic interactions. This loosening was further validated by analyzing the kinetic encapsulation strength through direct atomic contacts.

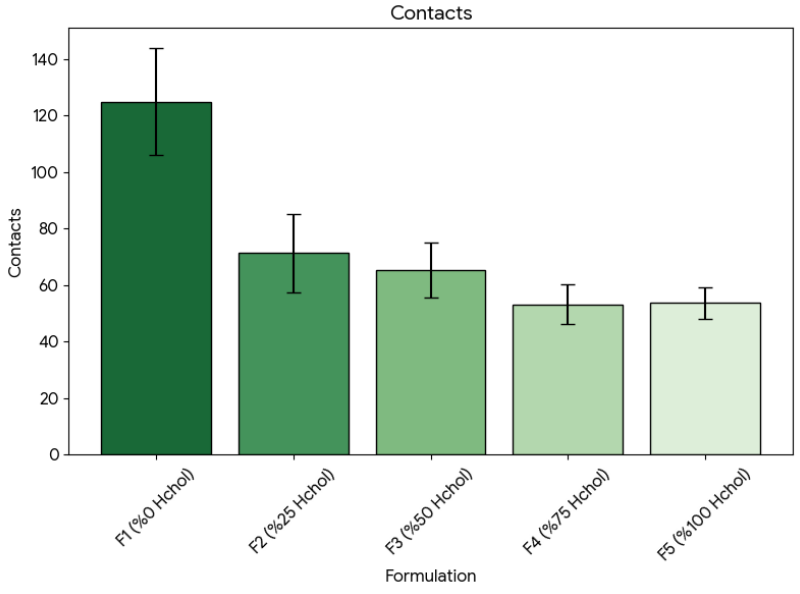

Figure 9. Time evolution of the number of direct atomic contacts (< 0.6 nm) between SM-102 lipids and the aptamer

As shown in Figure 9, the F1 system maintained an extremely rigid internal architecture with an average of 124.8±16.9 contacts. However, in the Hchol-integrated systems (F2 and F3), the number of direct SM102-aptamer contacts sharply decreased by approximately 40-45%. This strongly suggests a competitive binding environment where the cationic imidazole rings of Hchol actively share the electrostatic burden within the core. This targeted structural loosening at pH 4.0 acts as a "fusogenic primer"—it successfully destabilizes the overly rigid internal lipid network just enough to facilitate future endosomal membrane fusion and cytosolic release, without compromising the overall encapsulation.

Systemic Structural Integrity and Cargo Shielding at Physiological pH (7.4)

To confirm that the integration of the pH-responsive helper lipid (Hchol) does not compromise the structural integrity of the nanocarriers during systemic circulation, we evaluated the stability of the optimized F2 (25% Hchol) and F3 (50% Hchol) formulations at physiological pH (7.4). At this neutral pH, the imidazole headgroup of Hchol remains largely unprotonated, differentiating it from the highly cationic state induced by the acidic endosomal environment (pH 4.0).

Extended 1.0 μs molecular dynamics simulations (n=5) revealed that both F2 and F3 formulations maintain structural stability at pH 7.4 (Figure 10.). The morphological assessment showed that the LNPs preserved their stable vesicular-like architectures, exhibiting average *Rg* values of 11.90 ± 0.01 nm for F2 and 11.65 ± 0.03 nm for F3. These dimensions are highly consistent with the stable phase observed at pH 4.0, indicating that the particles do not undergo premature morphological collapse or erratic volumetric fluctuations in the bloodstream.

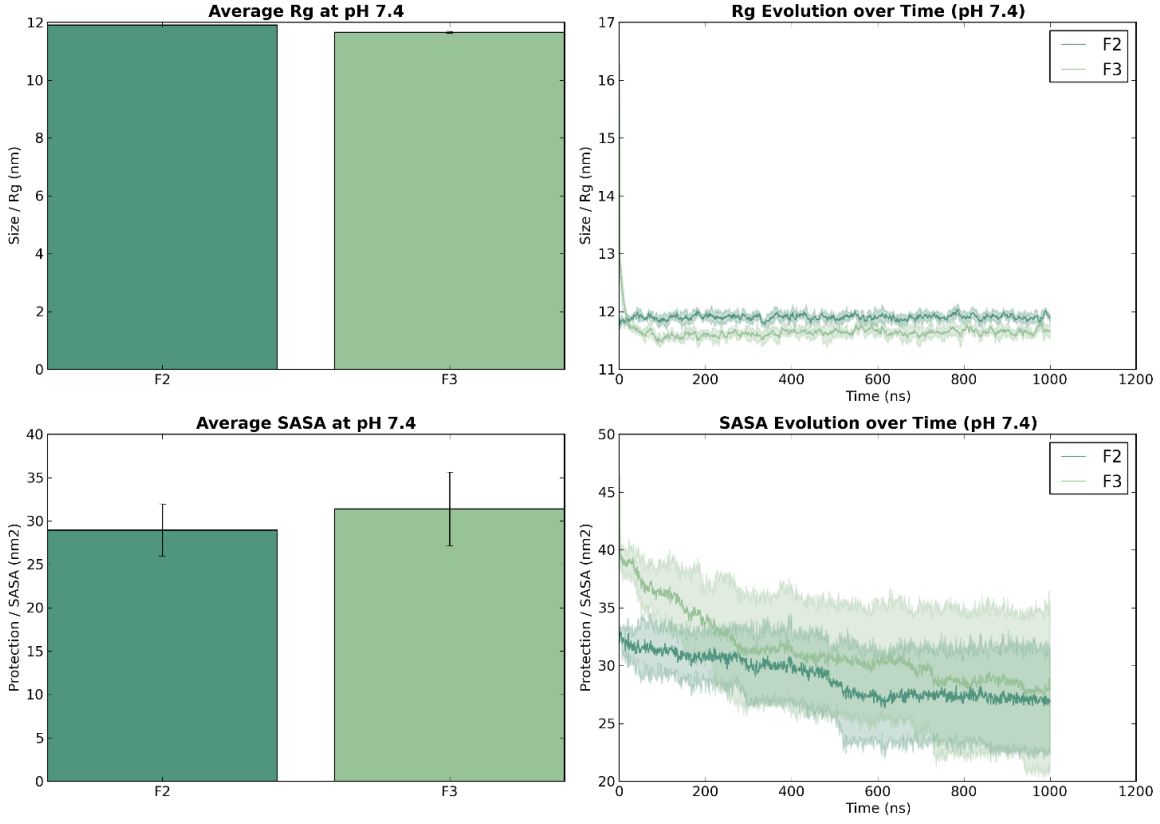

Figure 10. Structural and encapsulation stability of F2 and F3 formulations over 1.0 μs at pH 7.4

Crucially, the protective hydrophobic armor of the LNPs remained fully intact. The SASA of the encapsulated AS1411 aptamer stabilized at 28.96 ± 3.01 nm² for F2 and 31.40 ± 4.25 nm² for F3 (Table 2.). These values closely mirror the robust cargo compartmentalization observed in the acidic environment, unequivocally demonstrating that the internal water pool remains tightly sealed at pH 7.4. Consequently, these findings validate our hypothesis: the F2 and F3 formulations successfully resolve the stability-fusogenicity paradox by remaining structurally robust and protective during systemic circulation, while exclusively deploying their fusogenic VBC mechanism in response to targeted endosomal acidification.

Table 2. Quantitative Assessment of LNP Stability at Physiological pH (7.4). The percentages represent fractional substitutions within the total sterol content, not the entire LNP formulation

Formulation	Hchol Ratio / Number of Molecules	Radius of Gyration, *Rg* (nm)	Aptamer SASA (nm²)
F2	25% / 96 molecules	11.90 ± 0.01	28.96 ± 3.01
F3	50% / 192 molecules	11.65 ± 0.03	31.40 ± 4.25

Mechanistic insights: from proton sponge to VBC

The mechanistic role of Hchol has traditionally been attributed to the "proton sponge" effect, where imidazole protonation buffers endosomal pH, leading to osmotic swelling and membrane rupture. However, our data support a more nuanced, modern interpretation: the VBC mechanism proposed by Pei (2025). The critical finding in our RDF analysis is the 45% reduction in direct atomic contacts between the SM-102 ionizable lipids and the aptamer backbone in F2 and F3 formulations. In the control (F1), the protonated SM-102 lipids exert an intense "electrostatic grip" (RDF peak: 28.65), which has been identified by Pei (2025) as a primary rate-limiting step for cytosolic release.

The introduction of Hchol in F2 and F3 formulations reduced direct SM102-aptamer contacts by approximately 45%. We hypothesize that the cationic imidazole rings of Hchol competitively share the electrostatic burden, effectively "softening" the internal lipid network. This targeted structural loosening at pH 4.0 acts as a "fusogenic primer," facilitating the VBC mechanism (Pei, 2025). According to the VBC model, this allows ionizable lipids to more easily insert into the endosomal membrane, inducing negative membrane curvature and the subsequent budding of unstable vesicles that collapse to release the cargo into the cytosol (Dougherty, Sahni, & Pei, 2019; Pei, 2025).

The rational design of LNPs hinges on balancing extracellular structural stability with intracellular fusogenic activity. Our molecular dynamics titration reveals that the substitution of conventional cholesterol with the pH-responsive helper lipid Hchol triggers a fundamental remodeling of the LNP architecture, which has profound implications for endosomal escape and therapeutic efficacy (Trollmann, Rossetti, & Böckmann, 2025).

Sterol-mediated morphological phase transitions

The most striking observation in this study is the rapid morphological phase transition from a compact micellar core to a voluminous vesicular-like architecture upon the introduction of Hchol. In the control formulation (F1), the LNP maintained an exceptionally stable R_g of 4.61 nm, consistent with the dense, oil-droplet-like cores described in clinically approved siRNA-LNP systems (Trollmann & Böckmann, 2022). However, the substitution of just 25% of the sterol fraction with Hchol (F2) triggered a near-tripling of the R_g to 11.34 nm.

This expansion is biophysically driven by the protonation of the imidazole headgroups at pH 4.0. The transition from a neutral to a cationic state increases the effective "lipid packing parameter" due to electrostatic repulsion and increased hydration of the headgroup region. Our data demonstrate that while Hchol facilitates this fusogenic expansion, it cannot replace

the structural "scaffolding" role of conventional cholesterol. The total exclusion of standard cholesterol in the F5 system resulted in catastrophic structural instability, with erratic fluctuations between 5.1 and 8.8 nm. This confirms that a baseline ratio of rigid, non-ionizable sterols is mandatory to maintain the structural status and prevent premature collapse (Ramezanpour & Tieleman, 2022; Suzuki & Ishihara, 2021).

Cargo compartmentalization and protective integrity

A critical paradox in LNP development is that modifications enhancing fusogenicity often compromise the "hydrophobic armor" required to protect sensitive oligonucleotides like the AS1411 aptamer from nuclease-mediated degradation. Our SASA analysis provides conclusive evidence that Hchol-mediated expansion does not lead to cargo leakage. Despite the LNP volume increasing nearly five-fold, the aptamer's SASA remained strictly conserved between 25.15 and 28.66 nm^2.

This spatial density conservation mathematically proves that the internal water pool remains tightly sealed, and the cargo remains densely packed at the thermodynamic center of the nanoparticle. Furthermore, the structural topology of the G-quadruplex aptamer was perfectly preserved, with RMSD values hovering around 0.60 nm. This structural stability confirms that the native G-quadruplex topology of the AS1411 aptamer is preserved during core encapsulation, ensuring its therapeutic conformational integrity upon subsequent endosomal release into the cytoplasm.

CONCLUSION

This study provides a biophysical roadmap for the optimization of pH-responsive lipid nanoparticles. Through comprehensive molecular dynamics titration, we have identified a "Goldilocks" therapeutic window represented by the F2 (25% Hchol) and F3 (50% Hchol) formulations. Crucially, our simulations confirm that these intermediate titrations resolve the stability-fusogenicity paradox through a highly efficient dual-action mechanism. They maintain a robust, protective vesicular architecture during simulated systemic circulation (pH 7.4) to prevent premature cargo leakage, while exclusively undergoing the targeted internal electrostatic remodeling necessary to overcome the rate-limiting step of endosomal escape (Han et al., 2021) via the VBC mechanism at pH 4.0.

By coupling the intracellular therapeutic potential of the AS1411 aptamer with the pH-triggered escape dynamics of Hchol, we have defined a modular platform capable of bypassing the <5% delivery efficiency bottleneck of current LNP technologies. These findings establish the Hchol-modified LNP framework as a robust vehicle for the systemic stabilization and intracellular delivery of structurally sensitive nucleic acid therapeutics. Future investigations should focus on correlating these in silico findings with cell-based endosomal trafficking assays to validate the predicted increase in cytosolic bioavailability.

AUTHOR CONTRIBUTION STATEMENT

OK: conceptualization, methodology, investigation, data curation, formal analysis, visualization, writing – original draft, writing – review & editing, supervising. CY: conceptualization, writing – review & editing.

CONFLICT OF INTEREST

The authors declare that there is no conflict of interest.

REFERENCES

Abraham, M. J., Murtola, T., Schulz, R., Páll, S., Smith, J. C., Hess, B., & Lindah, E. (2015). GROMACS: High-performance molecular simulations through multi-level parallelism from laptops to supercomputers. *SoftwareX*, *1–2*, 19–25. https://doi.org/10.1016/J.SOFTX.2015.06.001

Bates, P. J., Laber, D. A., Miller, D. M., Thomas, S. D., & Trent, J. O. (2009). Discovery and development of the G-rich oligonucleotide AS1411 as a novel treatment for cancer. *Experimental and Molecular Pathology*, *86*(3), 151–164.

Burley, S. K., Berman, H. M., Kleywegt, G. J., Markley, J. L., Nakamura, H., & Velankar, S. (2017). Protein Data Bank (PDB): The Single Global Macromolecular Structure Archive. *Methods in Molecular Biology*, *1607*, 627–641. https://doi.org/10.1007/978-1-4939-7000-1_26

Bussi, G., Donadio, D., & Parrinello, M. (2007). Canonical sampling through velocity rescaling. *Journal of Chemical Physics*, *126*(1). https://doi.org/10.1063/1.2408420/186581

Cheng, Q., Wei, T., Jia, Y., Farbiak, L., Zhou, K., Zhang, S.,…Zhu, H. (2018). Dendrimer-Based Lipid Nanoparticles Deliver Therapeutic FAH mRNA to Normalize Liver Function and Extend Survival in a Mouse Model of Hepatorenal Tyrosinemia Type I. *Advanced Materials*, *30*(52), 1805308. https://doi.org/10.1002/ADMA.201805308

Cullis, P. R., & Hope, M. J. (2017). Lipid Nanoparticle Systems for Enabling Gene Therapies. *Molecular Therapy*, *25*(7), 1467–1475. https://doi.org/10.1016/J.YMTHE.2017.03.013

De Jong, D. H., Singh, G., Bennett, W. F. D., Arnarez, C., Wassenaar, T. A., Schäfer, L. V.,…Marrink, S. J. (2013). Improved parameters for the martini coarse-grained protein force field. *Journal of Chemical Theory and Computation*, *9*(1), 687–697. https://doi.org/10.1021/CT300646G/SUPPL_FILE/CT300646G_SI_001.PDF

Donahue, N. D., Acar, H., & Wilhelm, S. (2019). Concepts of nanoparticle cellular uptake, intracellular trafficking, and kinetics in nanomedicine. *Advanced Drug Delivery Reviews*, *143*, 68–96. https://doi.org/10.1016/J.ADDR.2019.04.008

Dougherty, P. G., Sahni, A., & Pei, D. (2019). Understanding Cell Penetration of Cyclic Peptides. *Chemical Reviews*, *119*(17), 10241–10287. https://doi.org/10.1021/acs.chemrev.9b00008

Eygeris, Y., Patel, S., Jozic, A., Sahay, G., & Sahay, G. (2020). Deconvoluting Lipid Nanoparticle Structure for Messenger RNA Delivery. *Nano Letters*, *20*(6), 4543–4549. https://doi.org/10.1021/ACS.NANOLETT.0C01386/ASSET/IMAGES/LARGE/NL0C01386_0005.JPEG

Gilleron, J., Querbes, W., Zeigerer, A., Borodovsky, A., Marsico, G., Schubert, U.,…Zerial, M. (2013). Image-based analysis of lipid nanoparticle–mediated siRNA delivery, intracellular trafficking and endosomal escape. *Nature Biotechnology, 31*(7), 638–646. https://doi.org/10.1038/nbt.2612

Han, X., Zhang, H., Butowska, K., Swingle, K. L., Alameh, M. G., Weissman, D., & Mitchell, M. J. (2021). An ionizable lipid toolbox for RNA delivery. *Nature Communications, 12*(1), 7233-. https://doi.org/10.1038/s41467-021-27493-0

Hassett, K. J., Benenato, K. E., Jacquinet, E., Lee, A., Woods, A., Yuzhakov, O.,…Brito, L. A. (2019). Optimization of Lipid Nanoparticles for Intramuscular Administration of mRNA Vaccines. *Molecular Therapy - Nucleic Acids*, *15*, 1–11. https://doi.org/10.1016/J.OMTN.2019.01.013

Hou, X., Zaks, T., Langer, R., & Dong, Y. (2021). Lipid nanoparticles for mRNA delivery. *Nature Reviews Materials, 6*(12), 1078–1094. https://doi.org/10.1038/s41578-021-00358-0

Jung, O., Jung, H.-Y, Thuy, L. T., Choi, M., Kim, S., Jeon, H. G.,…Choi, J. S. (2024). Modulating Lipid Nanoparticles with Histidinamide-Conjugated Cholesterol for Improved Intracellular Delivery of mRNA. *Advanced Healthcare Materials*, *13*(14), 2303857. https://doi.org/10.1002/ADHM.202303857

Kulkarni, J. A., Witzigmann, D., Leung, J., Tam, Y. Y. C., & Cullis, P. R. (2019). On the role of helper lipids in lipid nanoparticle formulations of siRNA. *Nanoscale*, *11*(45), 21733–21739. https://doi.org/10.1039/C9NR09347H

Kulkarni, J. A., Witzigmann, D., Thomson, S. B., Chen, S., Leavitt, B. R., Cullis, P. R., & van der Meel, R. (2021). The current landscape of nucleic acid therapeutics. *Nature Nanotechnology*, *16*(6), 630–643.

Miao, L., Li, L., Huang, Y., Delcassian, D., Chahal, J., Han, J.,…Anderson, D. G. (2019). Delivery of mRNA vaccines with heterocyclic lipids increases anti-tumor efficacy by STING-mediated immune cell activation. *Nature Biotechnology, 37*(10), 1174–1185. https://doi.org/10.1038/s41587-019-0247-3

Mitchell, M. J., Billingsley, M. M., Haley, R. M., Wechsler, M. E., Peppas, N. A., & Langer, R. (2020). Engineering precision nanoparticles for drug delivery. *Nature Reviews Drug Discovery, 20*(2), 101–124. https://doi.org/10.1038/s41573-020-0090-8

Patel, S., Ashwanikumar, N., Robinson, E., Xia, Y., Mihai, C., Griffith, J. P.,…Sahay, G. (2020). Naturally-occurring cholesterol analogues in lipid nanoparticles induce polymorphic shape and enhance intracellular delivery of mRNA. *Nature Communications, 11*(1), 983-. https://doi.org/10.1038/s41467-020-14527-2

Paunovska, K., Loughrey, D., & Dahlman, J. E. (2022). Drug delivery systems for RNA therapeutics. *Nature Reviews Genetics, 23*(5), 265–280. https://doi.org/10.1038/s41576-021-00439-4

Pei, D. (2025). Endosomal Escape of Lipid Nanoparticles: A Perspective on the Literature Data. *ACS Nano*, *19*(47), 40293–40303. https://doi.org/10.1021/ACSNANO.5C11721/ASSET/IMAGES/MEDIUM/NN5C11721_0008.GIF

Ramezanpour, M., & Tieleman, D. P. (2022). Computational Insights into the Role of Cholesterol in Inverted Hexagonal Phase Stabilization and Endosomal Drug Release. *Langmuir*, *38*(24), 7462–7471. https://doi.org/10.1021/ACS.LANGMUIR.2C00430/ASSET/IMAGES/LARGE/LA2C00430_0004.JPEG

Sahay, G., Alakhova, D. Y., & Kabanov, A. V. (2010). Endocytosis of nanomedicines. *Journal of Controlled Release*, *145*(3), 182–195. https://doi.org/10.1016/J.JCONREL.2010.01.036

Schoenmaker, L., Witzigmann, D., Kulkarni, J. A., Verbeke, R., Kersten, G., Jiskoot, W., & Crommelin, D. J. A. (2021). mRNA-lipid nanoparticle COVID-19 vaccines: Structure and stability. *International Journal of Pharmaceutics*, *601*, 120586. https://doi.org/10.1016/J.IJPHARM.2021.120586

Suzuki, Y., & Ishihara, H. (2021). Difference in the lipid nanoparticle technology employed in three approved siRNA (Patisiran) and mRNA (COVID-19 vaccine) drugs. *Drug Metabolism and Pharmacokinetics*, *41*, 100424. https://doi.org/10.1016/J.DMPK.2021.100424

Trollmann, M. F. W., & Böckmann, R. A. (2022). mRNA lipid nanoparticle phase transition. *Biophysical Journal*, *121*(20), 3927–3939. https://doi.org/10.1016/J.BPJ.2022.08.037

Trollmann, M. F. W., Rossetti, P., & Böckmann, R. A. (2025). Revisiting lipid nanoparticle composition and structure: A critical take on simulation approaches. *Proceedings of the National Academy of Sciences of the United States of America*, *122*(9), e2422995122. https://doi.org/10.1073/PNAS.2422995122/ASSET/E1220606-37C3-48F6-9344-EF54F9DEF74D/ASSETS/IMAGES/LARGE/PNAS.2422995122FIG01.JPG

Van den Avont, A., & Sharma-Walia, N. (2023). Anti-nucleolin aptamer AS1411: an advancing therapeutic. *Frontiers in Molecular Biosciences*, *10*, 1217769.

Vermeulen, L. M. P., De Smedt, S. C., Remaut, K., & Braeckmans, K. (2018). The proton sponge hypothesis: Fable or fact? *European Journal of Pharmaceutics and Biopharmaceutics*, *129*, 184–190. https://doi.org/10.1016/J.EJPB.2018.05.034

Wei, Z., Zhou, Y., Wang, R., Wang, J., & Chen, Z. (2022). Aptamers as Smart Ligands for Targeted Drug Delivery in Cancer Therapy. *Pharmaceutics, 14*(12). https://doi.org/10.3390/PHARMACEUTICS14122561

Yuan, S., Chan, H. C. S., & Hu, Z. (2017). Using PyMOL as a platform for computational drug design. *Wiley Interdisciplinary Reviews: Computational Molecular Science*, *7*(2), e1298. https://doi.org/10.1002/WCMS.1298

Zhu, G., & Chen, X. (2018). Aptamer-based targeted therapy. *Advanced Drug Delivery Reviews*, *134*, 65–78. https://doi.org/10.1016/J.ADDR.2018.08.005